RPLP0 drives diffuse large B-cell lymphoma cell proliferation through reactive oxygen species-dependent AKT/mTOR activation and inhibition of stress-induced autophagy

SHANSHAN WANG[1*], XUTAO YANG[1*], ROCHELLE MCGOWAN[2], BELINDA HODGE[2], DANIEL SHAN[2], NICOLAS MILLER[2] and JIAHONG TANG[1]

[1]Department of Hematology and Oncology, Hospital of Joint Logistics Support Force, Zhengzhou, Henan 450007, P.R. China; [2]Department of Genetics, DICAT National Biomedical Computation Centre, Vancouver BC V6B 5A6, Canada

Received April 21, 2026; Accepted July 7, 2026

DOI: 10.3892/etm.2026.13264

Abstract. Diffuse large B-cell lymphoma (DLBCL) is a common, aggressive subtype of non-Hodgkin lymphoma with poor outcomes. Identifying the primary molecular causes of DLBCL remains key. The present study examined the function of ribosomal protein lateral stalk subunit P0 (*RPLP0*) in DLBCL pathogenesis. The Cancer Genome Atlas-DLBCL and GSE12453 datasets overlapping differentially expressed genes were identified. Hub genes were identified via protein-protein interaction network analysis. DLBCL cells were subjected to functional tests following *RPLP0* overexpression or knockdown. Reverse transcription-quantitative PCR, western blotting, flow cytometry, transmission electron microscopy, colony formation assay and biochemical analysis were among the tests performed. N-acetylcysteine (NAC), rapamycin (RAPA) and 3-MA were among the medication therapies. In the DLBCL datasets, six ribosome-associated genes were differentially expressed. *RPLP0* knockdown inhibited the proliferation of DLBCL cells and caused G_2-phase arrest, without impacting apoptosis. Thioredoxin, heat shock protein family A member 1A and heat shock protein family B member 1 expression was downregulated by *RPLP0* knockdown, which also increased the NAD^+/NADH ratio, promoted reactive oxygen species (ROS) accumulation and caused mitochondrial membrane potential depolarization. Meanwhile, 3-MA reversed the effects of *RPLP0* knockdown, which encouraged LC3-II accumulation, autophagy-related gene 5 (*ATG5*) overexpression and an increase in autophagic vesicles. Autophagy-related indicators were decreased, and AKT/mTOR phosphorylation was increased by *RPLP0* overexpression, which RAPA inhibited. NAC therapy preserved the viability of *RPLP0*-silenced cells, restored p-AKT/p-mTOR levels and restored normal LC3 and ATG5 expression. These findings suggest that *RPLP0* regulates stress-induced autophagy through ROS-dependent AKT/mTOR signaling and may represent a potential therapeutic target for DLBCL.

Correspondence to: Dr Jiahong Tang, Department of Hematology and Oncology, Hospital of Joint Logistics Support Force, 602 Zhengshang Road, Zhengzhou, Henan 450007, P.R. China
E-mail: tangjiahong988@163.com

*Contributed equally

Key words: diffuse large B-cell lymphoma, *RPLP0*, autophagy, oxidative stress, AKT/mTOR signaling pathway

Introduction

Non-Hodgkin lymphoma (NHL) is a heterogeneous malignancy of the lymphatic system, and dozens of subtypes have been identified to date (1). With the aging of the global population, the incidence burden of NHL is expected to increase substantially, with the number of newly diagnosed cases projected to rise from ~545,000 cases in 2020 to 778,000 cases by 2040 (2). Among patients with NHL, 30-40% are of the most prevalent subtype, diffuse large B-cell lymphoma (DLBCL) (3). The incidence of DLBCL varies geographically and increases substantially with age, ranging from ~2.3 to 13.8 cases per 100,000 person-years (4). Elderly individuals, particularly those aged >60 years, are more frequently affected (5). Gene damage, epigenetic instability and long-term immunological activation all contribute to its etiology (6). Together, these elements alter interactions within the tumor microenvironment, B-cell differentiation and survival signal transduction. A notable portion of patients continue to develop primary resistance or relapse despite marked advancements in molecular profiling (7). Rituximab with cyclophosphamide, doxorubicin, vinblastine and prednisone is the standard first-line treatment (8). For high-risk disease subgroups, such as patients with aggressive biological characteristics or a poor response to immunochemotherapy, the results are still disappointing (9).

A notable factor influencing stress adaptation in cancer is autophagy, a conserved lysosome-dependent catabolic process (10). Autophagy promotes metabolic flexibility, limits oxidative stress and modifies immune-related signals by removing damaged organelles and protein aggregates (11). Impaired autophagy has been associated with worse outcomes following immunochemotherapy in DLBCL. According

to Xu *et al* (12) the paired box 5-driven long non-coding RNA (lncRNA) ARRDC1-AS1 enhances autophagy by regulating autophagy-related gene 5 (ATG5) through the sequestration of microRNA-2355-5p, thereby promoting the development of DLBCL. Furthermore, research suggests that the combination of rituximab and chidamide might reduce treatment resistance by increasing the expression of autophagy-associated proteins (13). By specifically regulating the stability of carcinogenic signaling proteins, autophagy can also be involved in the biological processes of DLBCL. In the MCD subtype of DLBCL, characterized by $MYD88^{L265P}$ and CD79B mutations, TANK-binding kinase 1 (*TBK1)*-dependent selective autophagy can target and degrade the ubiquitinated $MYD88^{L265P}$ protein, and bruton tyrosine kinase (BTK) inhibitors appear to enhance this autophagic clearance, potentially leading to therapeutic benefits (14). All of these outcomes point to autophagy as a therapeutically useful and physiologically marked process in DLBCL.

A fundamental member of the ribosomal P protein family, ribosomal protein lateral stalk subunit P0 (*RPLP0*), is necessary for ribosome stability and translational elongation (15). There is growing evidence that numerous cancer types, such as lung and prostate cancer, exhibit abnormal expression of *RPLP0* (16,17). The clinical prognosis and tumor progression are intimately linked to this imbalance. Reactive oxygen species (ROS) accumulate as a result of inhibition of RPLP family proteins, which initiates autophagy, reduces proliferation and induces G_2 phase arrest, according to findings (18). These findings suggest that *RPLP0*-associated translational processes regulate autophagy and redox homeostasis in cancer cells. The PI3K/AKT/mTOR signaling cascade is a key oncogenic hub that integrates cellular stress, growth factor signals and nutrient availability (19). While PI3K/AKT/mTOR activation typically inhibits autophagic activity, pathway inhibition might increase autophagic flux and encourage cell death. The data presented suggest that *RPLP0* may influence autophagy in DLBCL via the PI3K/AKT/mTOR pathway, with implications for biomarker development and patient stratification.

DLBCL may develop due to oxidative stress and altered mitochondrial activity, according to prior research (20,21). The autophagy system helps maintain cellular homeostasis under stressful conditions. Moreover, the AKT/mTOR signaling pathway is known to regulate cell survival and autophagy in response to environmental cues. The aim of the present study was to clarify the role of *RPLP0* in regulating these cellular processes in DLBCL. Based on the aforementioned evidence, we hypothesized that *RPLP0* promotes DLBCL cell survival by maintaining redox homeostasis and activating the AKT/mTOR pathway, thereby suppressing stress-induced autophagy. Investigating these pathways will shed light on the molecular causes of DLBCL and may reveal potential therapeutic targets.

Materials and methods

Data selection and differential expression analysis. The Gene Expression Omnibus Database (https://www.ncbi.nlm.nih.gov/gds/) and The Cancer Genome Atlas (TCGA) database (https://www.cancer.gov/ccg/research/genome-sequencing/tcga) provided the gene expression data for this present investigation. TCGA-DLBC dataset was selected, which includes 48 DLBCL tumor samples from TCGA and 929 normal control samples from the Genotype-Tissue Expression database (https://gtexportal.org/), and the GSE12453 dataset, containing 11 tumor samples and 25 normal samples (22). Differential expression analysis of genes in the two datasets was performed using the R package 'Limma' (version 3.54.2; Bioconductor; T Core Team) (23). Genes were screened based on fold change (FC), with FC>2 considered as upregulated differentially expressed genes (DEGs) and FC<0.5 considered as downregulated DEGs, with a significance criterion of $P<0.05$. Intersection analysis was then performed on the upregulated and downregulated DEGs to obtain key intersection genes utilizing Bioinformatics & Evolutionary Genomics (https://bioinformatics.psb.ugent.be/webtools/Venn/).

Protein-protein interaction (PPI) network and selection of hub genes. To assess the potential functional relevance of key intersecting genes, the authors analyzed the STRING database (https://string-db.org/) to construct a PPI network. The top 15 genes were further analyzed for their interaction networks using the Module Clustering Coefficient (MCC), Edge Percolated Component (EPC) and Maximum Neighborhood Component (MNC) algorithms in the CytoHubba plugin of Cytoscape software (version 3.10.1; Cytoscape Consortium). Subsequently, the top 15 genes from these three algorithms were subjected to intersection analysis to obtain candidate genes. Then, gene expression analysis of these candidate genes was performed on TCGA-DLBC and GSE12453 datasets using the Sanger website (http://vip.sangerbox.com/home.html). By analyzing gene expression levels in the normal and tumor groups, the present study identified the pivotal genes.

Cell culture. Human normal lymphoblastic GM12878 and DLBCL cell lines (OCI-LY7 and U2932) were acquired from Changsha Abiwei Biotechnology Co., Ltd. and the DLBCL cell line OCI-LY8 was purchased from Shanghai Enzyme-linked Biotechnology Co., Ltd. OCI-LY8 cells were cultured in DMEM medium (Gibco; Thermo Fisher Scientific, Inc.). GM12878, OCI-LY7 and U2932 cells were cultured under the same conditions in RPMI 1640 medium (Gibco; Thermo Fisher Scientific, Inc.). In all media, 10% fetal bovine serum (Gibco; Thermo Fisher Scientific, Inc.) and 1% penicillin-streptomycin (Gibco; Thermo Fisher Scientific, Inc.) were included. The cells were cultivated in an incubator with 5% CO_2 at 37˚C for 24 h before subsequent experiments.

Cell transfection and treatment. Lipofectamine 2000 (Invitrogen; Thermo Fisher Scientific, Inc.) was used for cell transfection in accordance with the manufacturer's recommendations. For *RPLP0* knockdown studies, cells were transfected with three *RPLP0*-specific small interfering RNAs (siRNAs): si-*RPLP0*-1 (sense, 5'-GCUAAGGUUGAAGCCAAGGAA-3'; and antisense, 5'-UUCCUUGGCUUCAACCUUAGC-3'), si-*RPLP0*-2 (sense, 5'-UGAUCAAGACUGGAGACAAAG-3' and antisense, 5'-CUUUGUCUCCAGUCUUGAUC-3') and si-*RPLP0*-3 (sense, 5'-GCUGCUGAACAUGCUCAACAU-3' and antisense, 5'-AUGUUGAGCAUGUUCAGCCAGC-3') or a non-targeting control siRNA (si-NC; sense, 5'-UUCUCCGAACGUGUCACGUTT-3' and

antisense, 5'-ACGUGACACGUUCGGAGAATT-3') at a final concentration of 50 nM. For overexpression studies, cells were transfected with the corresponding empty vector or a pcDNA3.1(+)-*RPLP0* expression plasmid generated using the pcDNA3.1(+) backbone (Invitrogen; Thermo Fisher Scientific, Inc.) with 2 μg plasmid DNA used per well in a 6-well plate. The plasmid construct was verified by DNA sequencing. For subsequent investigations, cells were harvested 48 h after transfection.

DLBCL cells require special treatment for autophagy studies. 3-Methyladenine (3-MA; Sigma-Aldrich; Merck KGaA) is an autophagy inhibitor that acts in the early stages of the autophagy pathway. To block autophagy, DLBCL cells were treated with 10 mM 3-MA for 48 h. Rapamycin (RAPA) is a typical mTOR inhibitor. DLBCL cells were treated with 25 nM RAPA (Sigma-Aldrich; Merck KGaA) for 24 h for further analysis. A traditional ROS scavenger, N-acetyl-L-cysteine (NAC; Sigma-Aldrich; Merck KGaA), lowers intracellular ROS levels by directly interacting with ROS through redox processes. To regulate ROS levels, DLBCL cells were treated with 5 mM NAC for 2 h before subsequent assays.

Reverse transcription-quantitative PCR (RT-qPCR). Total RNA was extracted from OCI-LY7 and OCI-LY8 cells in the indicated treatment groups using TRIzol® reagent (Takara Bio, Inc.). Important procedures, including qPCR amplification, cDNA synthesis and RNA quality assessment, were carried out in accordance with the techniques outlined in earlier research (24). Specifically, cDNA was synthesized using the PrimeScript RT reagent Kit with gDNA Eraser (Takara Bio, Inc.). The reaction procedure included the removal of genomic DNA at 42˚C for 2 min, followed by reverse transcription at 37˚C for 15 min, and enzyme inactivation at 85˚C for 5 sec. qPCR amplification was performed using TB Green Premix Ex Taq II (Takara Bio, Inc.). The thermocycling conditions were as follows: Initial denaturation at 95˚C for 30 sec, followed by 40 cycles of denaturation at 95˚C for 5 sec and annealing/extension at 60˚C for 30 sec. Primer sequences are as follows: *RPLP0*: Forward: 5'-CGTCCTCGTGGAAGT GACAT-3', reverse: 5'-CTTGGAGCCCACATTGTCTG-3', *GAPDH*: forward: 5'-CATGTTGCAACCGGGAAGGA-3', reverse: 5'-ATCACCCGGAGGAGAAATCG-3'. mRNA expression was normalized using the endogenous reference *GAPDH*. The $2^{-\Delta\Delta Cq}$ method was employed for relative quantification (25).

Western blotting (WB). RIPA lysis buffer (Beyotime Biotechnology) containing phosphatase and protease inhibitors was used to extract total protein from cells. Following determination of protein content using a BCA Protein Assay Kit (Beyotime Biotechnology), in accordance with procedures described in previous studies, 30 μg of protein per lane was separated using 8-15% SDS-PAGE gels according to the molecular weights of the target proteins and transferred onto polyvinylidene fluoride membranes. The membranes were blocked with 5% bovine serum albumin for 1 h at room temperature in Tris-buffered saline containing 0.1% Tween-20 (TBST) (26). The membranes were incubated overnight with the primary antibody at 4˚C. The following are the primary antibodies utilized in this investigation: RPLP0 (cat. no. ab192866; 1:1,000), thioredoxin (TXN; cat. no. ab133524; 1:10,000), heat shock protein family A member 1A (HSPA1A; cat. no. ab5439; 1:1,000), heat shock protein family B member 1 (HSPB1; cat. no. ab2790; 1:1,000), microtubule-associated protein 1 light chain 3 alpha (MAP1LC3A; cat. no. ab52628; 1:50,000), ATG5 (cat. no. ab108327; 1:1,000), cleaved caspase-3 (cat. no. ab32351; 1:2,000), caspase-3 (cat. no. ab184787; 1:2,000), phosphorylated (p)-AKT1 (cat. no. 66444-1-Ig; 1:2,000), AKT1 (cat. no. 10176-2-AP; 1:2,000), p-mTOR (cat. no. ab109268; 1:1,000), mTOR (cat. no. ab109268; 1:1,000) and GAPDH (cat. no. ab181602; 1:10,000). Among them, p-AKT1 and AKT1 antibody were derived from Wuhan Sanying Biotechnology. By contrast, the other primary antibodies were derived from Abcam. Following three washes with TBST containing 0.1% Tween-20, the membrane was incubated for 1 h at room temperature with goat anti-rabbit (cat. no. ab6721; 1:2,000; Abcam) and anti-mouse secondary antibodies (cat. no. ab6789; 1:2,000; Abcam) conjugated to horseradish peroxidase. Immobilon Western Chemiluminescent HRP Substrate (Merck KGaA) was used for chemiluminescent detection. Image Lab software (version 6.1; Bio-Rad Laboratories, Inc.). was installed to measure band intensity.

Colony formation assay. OCI-LY7 and OCI-LY8 cells were transfected with si-NC or si-*RPLP0*-1. Following transfection, cells in the logarithmic growth phase were collected, resuspended in complete culture medium, and seeded into 6-well plates at a density of $1x10^3$ cells per well. The cells were cultured at 37˚C in a humidified atmosphere containing 5% CO_2 for 14 days, with the culture medium replaced every 3 days. After incubation, 4% paraformaldehyde was added to fix the cells for 15 min. After fixation, colonies were stained with nitroblue tetrazolium chloride for 30 min at room temperature. A cell cluster containing at least 50 cells was defined as a colony. Images were acquired using a chemiluminescence imaging system (Bio-Rad Laboratories, Inc.), and the colonies were counted using ImageJ software (version 1.53; National Institutes of Health).

Cell Counting Kit-8 (CCK-8) assay. 96-well plates were seeded with DLBCL cells at a density of 1,000 cells per well. After cell collection, 10 μl CCK-8 reagent (Dojindo Laboratories, Inc.) was added to 100 μl culture medium. After 2 h incubation at 37˚C, an iMark™ Microplate Absorbance Reader (Bio-Rad Laboratories, Inc.) was employed to quantify the optical density (OD) at 450 nm to identify cell growth.

Flow cytometry. As directed by the manufacturer, apoptosis was measured with an Annexin V-FITC/PI apoptosis detection kit (cat. no. ab14085; Abcam). Briefly, OCI-LY7 and OCI-LY8 cells were collected, cleaned in cold PBS and then reconstituted in 500 μl of 1X binding buffer. Annexin V-FITC (5 μl) was used to stain the cells at room temperature for 10 min in the dark, followed by PI (5 μl) for 5 min. Samples were analyzed on a FACSCalibur flow cytometer (BD Biosciences). Flow cytometric data were analyzed using FlowJo software (version 10.8.1; BD Biosciences).

For cell cycle analysis, cells were collected and fixed in pre-chilled 70% ethanol at -20˚C overnight. Following fixation, cells were washed with PBS, treated with RNase A

(100 μg/ml), and stained with PI (50 μg/ml) for 30 min in the dark. A FACSCalibur flow cytometer was used to quantify DNA content, and the proportions of cells in different cell cycle phases were analyzed using FlowJo software (version 10.8.1; BD Biosciences).

Mitochondrial membrane potential (MMP) assay. A JC-1 staining kit (cat. no. ab113850; Abcam) was used to assess MMP in OCI-LY7 and OCI-LY8 cells according to the manufacturer's instructions. Cells were cultured with the JC-1 working solution for 20 min at 37˚C in the dark after the specified treatments. Following incubation, the cells were immediately examined under a fluorescence microscope (Nikon Corporation) after being cleaned with PBS. Red JC-1 aggregates indicate intact $\Delta\Psi$m, whereas increased green JC-1 monomers reflect mitochondrial depolarization.

ROS level assay. 2',7'-dichlorodihydrofluorescein diacetate (DCFH-DA; Beyotime Biotechnology) was used to measure intracellular ROS levels in accordance with the manufacturer's directions. OCI-LY7 and OCI-LY8 cells were transfected with si-*RPLP0*-1 or si-NC, seeded on coverslips in 6-well plates, and incubated under standard culture conditions. Following the specified incubation period, cells were treated with DCFH-DA solution (10 μM) for 20 min in the dark at 37˚C after being rinsed with serum-free media. Excess probe was removed by washing three times with serum-free medium. DAPI (1 μg/ml) for 5 min was used to counterstain the nuclei, and a fluorescence microscope (Nikon Corporation) was used to capture fluorescence images rapidly.

Transmission electron microscope (TEM). Cells with si-NC or si-*RPLP0*-1 were collected and fixed in 2.5% glutaraldehyde overnight at 4˚C. Following a phosphate buffer wash, cells were dehydrated by a graded ethanol series, post-fixed for 1 h with 1% osmium tetroxide, and then embedded in epoxy resin. The resin blocks were polymerized at 60˚C for 48 h before ultrathin sectioning. After cutting and mounting ultrathin slices (70 nm thick) on copper grids, they were sequentially stained with 2% uranyl acetate for 15 min and lead citrate for 10 min at room temperature. Mitochondrial morphology was observed with an HT7700 TEM (Hitachi Ltd.).

Determination of NAD^+/NADH ratio. Intracellular NAD^+/NADH ratios were measured using a commercial NAD^+/NADH Assay Kit (cat. no. S0175, Beyotime Biotechnology) as directed by the manufacturer. Briefly, cells were harvested and lysed on ice in the NAD^+/NADH extraction buffer provided in the kit. The supernatants were collected after centrifuging the lysates at 12,000 x g for 10 min at 4˚C. For total NAD (NAD^+ + NADH) measurement, an aliquot of each extract was directly subjected to the enzymatic cycling reaction. To assess NADH, a parallel aliquot was chilled on ice after a 30 min incubation at 60˚C to break down NAD^+. Reaction mixtures were prepared according to the kit protocol, and absorbance at 450 nm was measured using an iMark microplate reader (Bio-Rad Laboratories, Inc.). NAD^+ levels were assessed as total NAD minus NADH, and the NAD^+/NADH ratio was computed as (total NAD-NADH)/NADH. Values were normalized to equal cell numbers (or total protein) across samples.

Statistical analysis. The R program (version 4.1.0; Posit Software, PBC) was used for the statistical analysis. Statistical significance was defined as $P<0.05$. Differences between groups were assessed using an unpaired Student's t-test (two groups), and one-way ANOVA with Tukey's post hoc test were employed to compare multiple groups. Each experiment was conducted at least three times, and the mean ± SD was used to describe the results.

Results

Identification and characterization of hub overlapping DEGs in DLBCL. In the present study, 6,338 upregulated and 1,115 downregulated DEGs were first identified from TCGA-DLBCL dataset (Fig. 1A). Additionally, from the GSE12453 dataset, 604 upregulated and 18 downregulated DEGs were detected (Fig. 1B). Venn diagram analysis was performed to identify overlapping DEGs between the two datasets, revealing 396 upregulated DEGs and 0 downregulated DEGs (Fig. 1C and D). PPI network analyses of these overlapping upregulated DEGs were conducted using the MCC, MNC and EPC algorithms. This analysis identified the top 15 most highly associated genes for each algorithm (Fig. 1E-G). Among these, six candidate genes (*RPS11*, *RPL27*, *RPS18*, *RPS5*, *RPLP0* and *RPS3*) were selected as potential biomarkers (Fig. 1H). Expression analysis of these candidate genes in DLBCL-related datasets revealed that, compared with normal controls, all six genes exhibited notably higher expression in the tumor group (Fig. 1I and J). The present investigation examined *RPLP0* because it is an essential component of the large ribosomal subunit and vital for protein synthesis.

Expression and knockdown efficiency of RPLP0 in DLBCL cell lines. The GM12878 cell line and DLBCL cell lines (OCI-LY7, OCI-LY8 and U2932) were subjected to RT-qPCR and WB analyses to assess RPLP0 levels in DLBCL. The results showed that *RPLP0* expression was elevated in DLBCL cell lines, with OCI-LY7 and OCI-LY8 cells exhibiting the highest levels (Fig. 2A-C). Three distinct siRNA constructs targeting *RPLP0* were transfected into OCI-LY7 and OCI-LY8 cells to investigate the function of *RPLP0*. *RPLP0* knockdown markedly reduced RPLP0 mRNA and protein levels by RT-qPCR and WB analyses, with si-*RPLP0*-1 showing the most effective knockdown (Fig. 2D-H).

RPLP0 knockdown disrupts proliferation, cell cycle and apoptosis in DLBCL cell lines. Colony formation assays assessed the effects of *RPLP0* knockdown on cell proliferation. The findings showed that, compared with the control group, silencing *RPLP0* reduced the ability of OCI-LY7 and OCI-LY8 cells to proliferate (Fig. 3A and B). The effects of *RPLP0* knockdown on the cell cycle distribution of OCI-LY7 and OCI-LY8 cells were next evaluated by flow cytometry. The outcomes revealed a concurrent build-up of cells in the G_2 phase and a notable decline in the proportion of cells in the S phase (Fig. 3C and D). Additionally, apoptosis experiments were conducted to determine if *RPLP0* knockdown affected cell death. However, there were no appreciable variations in the rates of apoptosis between the si-NC control group and the *RPLP0* knockdown group in DLBCL cell lines (Fig. 3E and F).

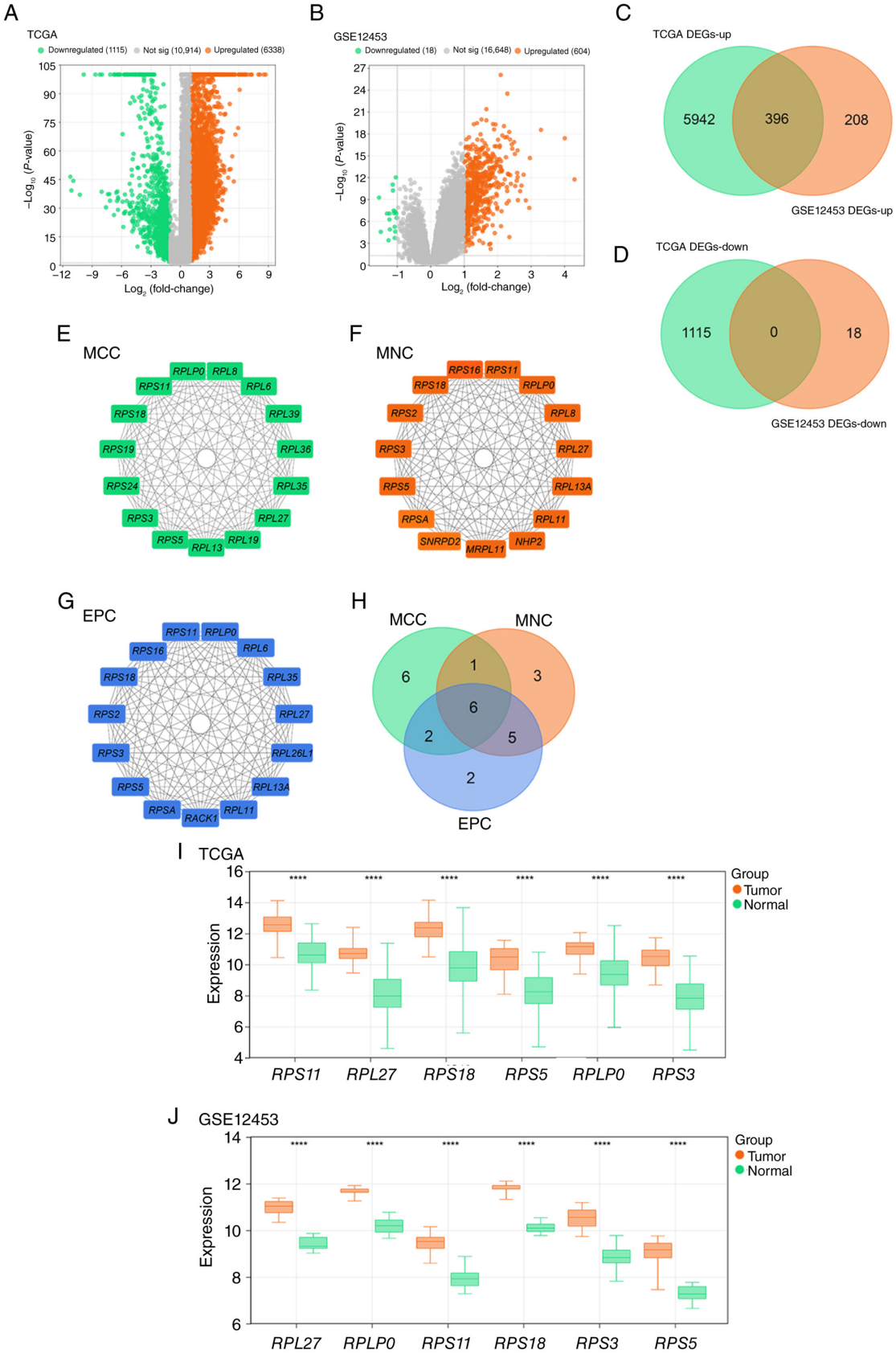

Figure 1. Overlapping DEGs in DLBCL found in the GSE12453 and TCGA-DLBCL datasets. (A) A volcano plot shows the upregulated (orange) and downregulated (green) DEGs from TCGA-DLBCL dataset. (B) The volcano plot shows the upregulated (orange) and downregulated (green) DEGs found in the GSE12453 dataset. (C) Venn diagram showing the overlap of upregulated DEGs between TCGA-DLBCL and GSE12453 datasets. (D) Venn diagram illustrating the overlap of downregulated DEGs between the two datasets. PPI network analysis of the overlapping upregulated DEGs. The top 15 genes were selected using the (E) MCC, (F) MNC and (G) EPC algorithms. (H) The six candidate genes were identified from the MCC, MNC and EPC algorithms. (I and J) Expression of the six candidate genes (*RPS11*, *RPL27*, *RPS18*, *RPS5*, *RPLP0* and *RPS3*) in DLBCL and normal groups in the (I) TCGA-DLBCL dataset and (J) GSE12453 datasets. ****P<0.0001. DLBCL, diffuse large B-cell lymphoma; DEGs, differentially expressed genes; PPI, protein-protein interaction; MCC, maximal clique centrality; MNC, maximum neighborhood component; EPC, edge percolated component; TCGA, The Cancer Genome Atlas.

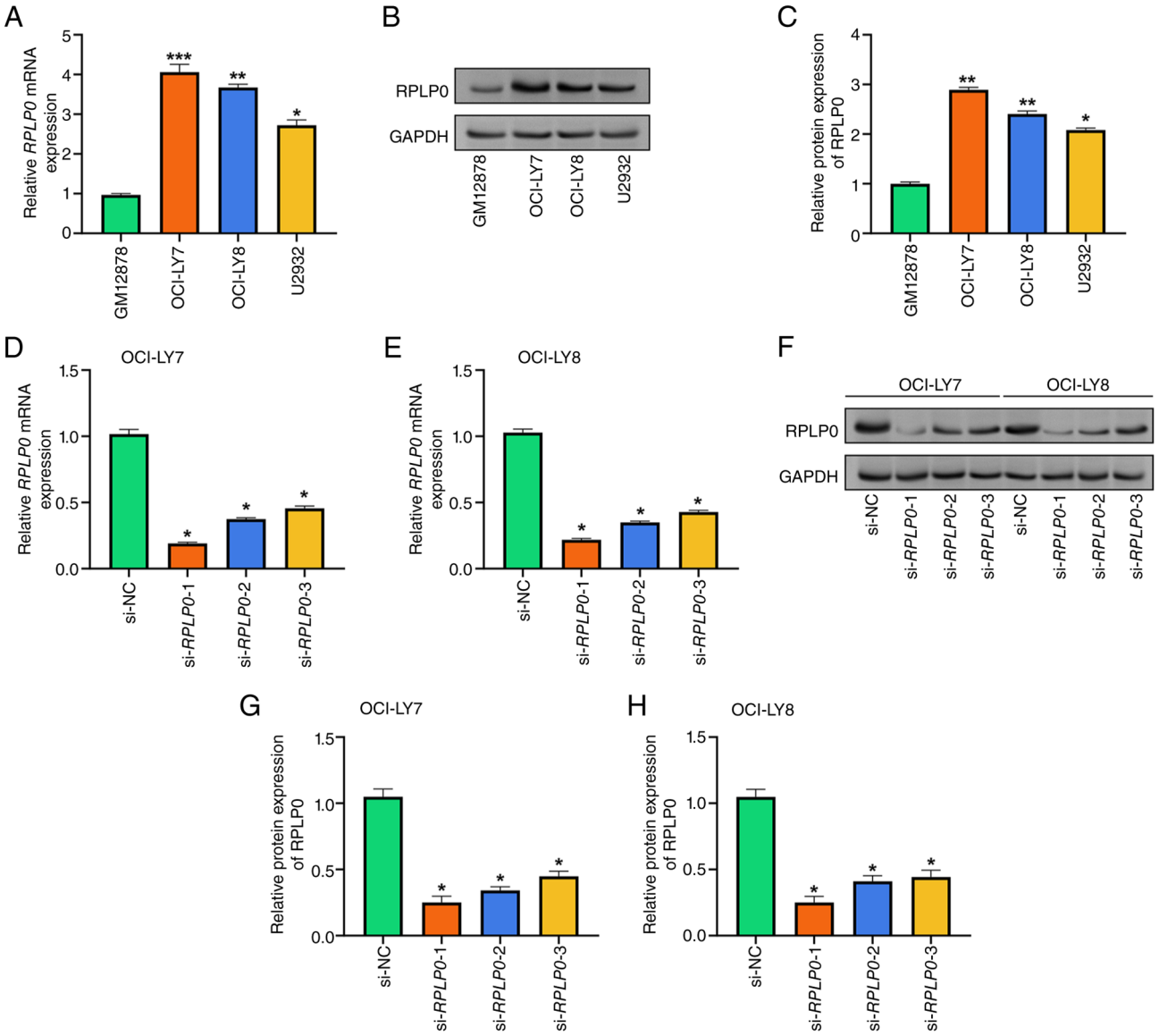

Figure 2. Expression and knockdown efficiency of *RPLP0* in DLBCL cell lines. (A) RT-qPCR analysis of *RPLP0* expression in the GM12878 (normal B cell), OCI-LY7, OCI-LY8 and U2932 cell lines. (B and C) WB analysis of RPLP0 expression in the GM12878 (normal B cell), OCI-LY7, OCI-LY8 and U2932 cell lines. Knockdown of *RPLP0* using three different siRNA constructs (si-*RPLP0*-1, si-*RPLP0*-2 and si-*RPLP0*-3) in (D) OCI-LY7 and (E) OCI-LY8 cells. The efficiency of *RPLP0* knockdown was assessed by RT-qPCR. The x-axis represents the siRNA constructs used (si-*RPLP0*-1, si-*RPLP0*-2 and si-*RPLP0*-3), and the y-axis shows relative mRNA levels. (F) The efficiency of *RPLP0* knockdown was assessed by WB. The y-axis shows relative protein levels in (G) OCI-LY7 and (H) OCI-LY8. *P<0.05, **P<0.01 and ***P<0.001. DLBCL, diffuse large B-cell lymphoma; RT-qPCR, reverse transcription-quantitative PCR; WB, western blot; si, small interfering RNA; NC, negative control.

These outcomes imply that *RPLP0* mainly controls DLBCL cell proliferation through cell cycle modulation.

RPLP0 knockdown disrupts redox homeostasis and induces mitochondrial dysfunction in DLBCL cells. The impact of *RPLP0* knockdown on oxidative damage repair markers in DLBCL cell lines was further examined. According to WB analysis, si-*RPLP0*-1 markedly decreased TXN, HSPA1A and HSPB1 protein expression compared with the control group (Fig. 4A-C). This is supported by the notable increase in the NAD^{+}/NADH ratio following *RPLP0* knockdown (Fig. 4D). Next, the authors utilized JC-1 staining to measure MMPs. Cells with silenced *RPLP0* showed decreased JC-1 aggregates and increased JC-1 monomers, indicating mitochondrial depolarization. Quantitative analysis of the red/green fluorescence ratio further confirmed a marked reduction in membrane potential compared with the si-NC group (Fig. 4E-F). Additionally, the si-*RPLP0*-1 group exhibited greater green fluorescence intensity in DCFH-DA staining, and quantitative analysis of ROS fluorescence intensity revealed a marked increase, suggesting enhanced intracellular ROS accumulation (Fig. 4G-H). These outcomes imply that *RPLP0* deficiency worsens mitochondrial function and oxidative damage in DLBCL cells.

RPLP0 deletion alters autophagy regulation and mitochondrial morphology in DLBCL cells. The transformation of LC3-I into LC3-II is a crucial stage in the creation of autophagosomes. In OCI-LY7 and OCI-LY8 cells transfected with si-*RPLP0*-1, the protein levels of LC3 and ATG5 were

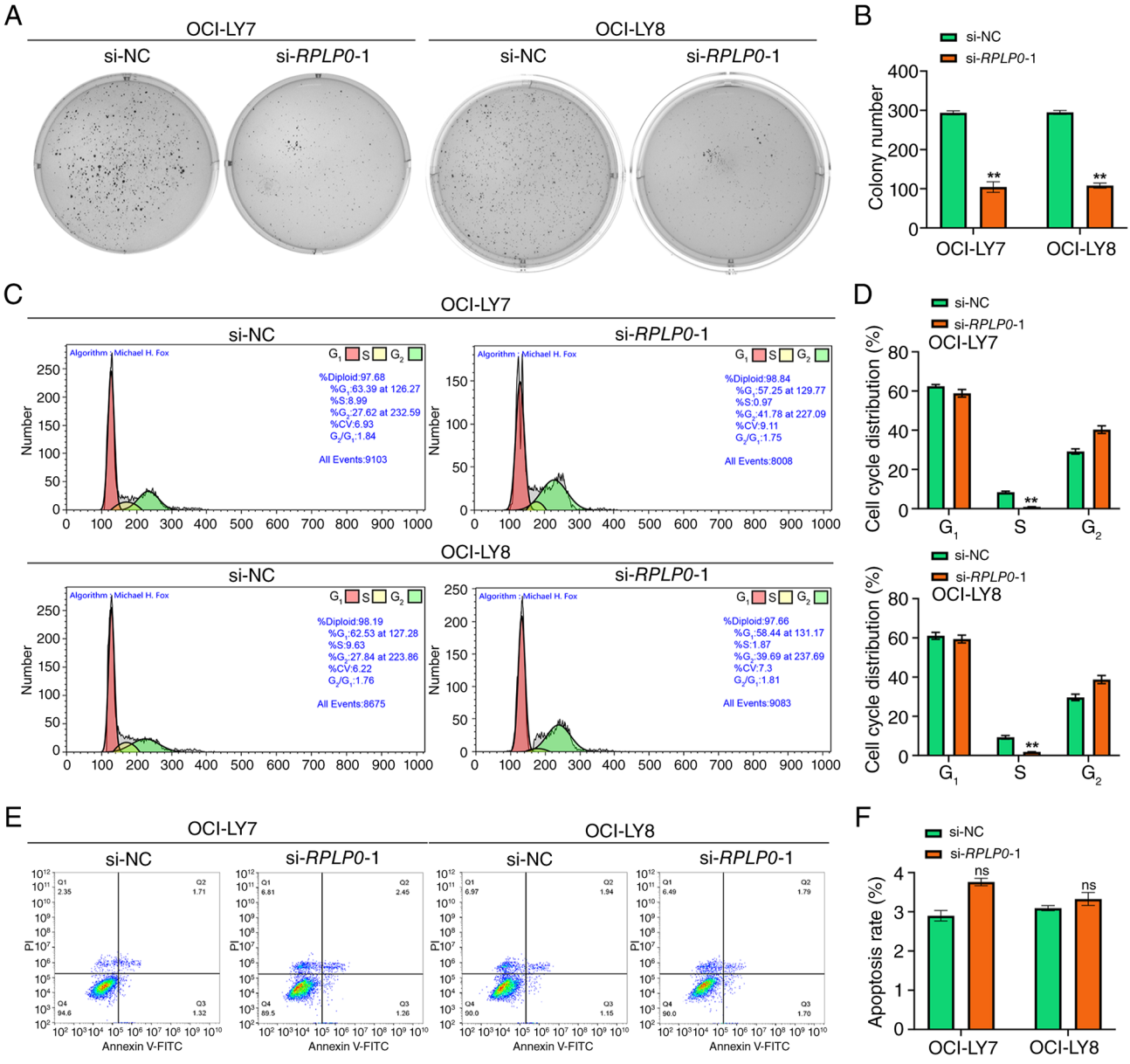

Figure 3. Effects of *RPLP0* knockdown on cell proliferation, cell cycle distribution and apoptosis in OCI-LY7 and OCI-LY8 cell lines. (A) Colony formation assay assessing the proliferative capacity of OCI-LY7 and OCI-LY8 cells following *RPLP0* knockdown. (B) The x-axis represents the different groups (si-NC vs. si-*RPLP0*-1) and the y-axis shows the number of colonies formed. (C) Cell cycle analysis by flow cytometry in OCI-LY7 and OCI-LY8 cells after *RPLP0* knockdown. (D) The x-axis represents the cell cycle phases (G_1, S and G_2), and the y-axis represents the percentage of cells in each phase. (E) Apoptosis analysis by flow cytometry in OCI-LY7 and OCI-LY8 cells after *RPLP0* knockdown. (F) Quantification of the apoptosis rate in the indicated groups (si-NC, si-*RPLP0*-1). **P<0.01. ns, not significant; si, small interfering RNA; NC, negative control; RPLP0, ribosomal protein lateral stalk subunit P0.

measured using WB to investigate the effect of *RPLP0* knockdown on autophagy. The present findings demonstrated that *RPLP0* knockdown increased the LC3-II/I ratio and upregulated ATG5 protein expression in both cell lines (Fig. 5A-C). TEM was subsequently used to examine the mitochondrial morphology of *RPLP0*-silenced cells. The findings revealed notable signs of autophagy, including an increase in the number of autophagic vacuoles in the field of view and quantification confirmed a notable increase in the number of autolysosomes per field (Fig. 5D and E). Next, the autophagy inhibitor 3-MA (5 mM) was added to *RPLP0*-silenced OCI-LY7 and OCI-LY8 cells. According to WB analysis, *RPLP0* knockdown increased the LC3-II/I ratio but had no discernible effect on caspase-3 expression. Nevertheless, 3-MA treatment reversed the effects of *RPLP0* knockdown, obviously reducing the LC3-II/I ratio and upregulating cleaved caspase-3 expression (Fig. 5F-H). The present findings suggest that *RPLP0* knockdown increases autophagy in DLBCL cells by modulating ATG5 and LC3-II expression.

Overexpression of RPLP0 activates AKT/mTOR signaling and inhibits autophagy in DLBCL cells. The transfection efficiency of the *RPLP0* overexpression plasmid was evaluated via RT-qPCR and WB in subsequent experiments. Investigations demonstrated that levels of *RPLP0* mRNA and protein expression of both cell lines were markedly increased after *RPLP0* overexpression (Fig. 6A-C). The effects of *RPLP0* overexpression on total and phosphorylated AKT and

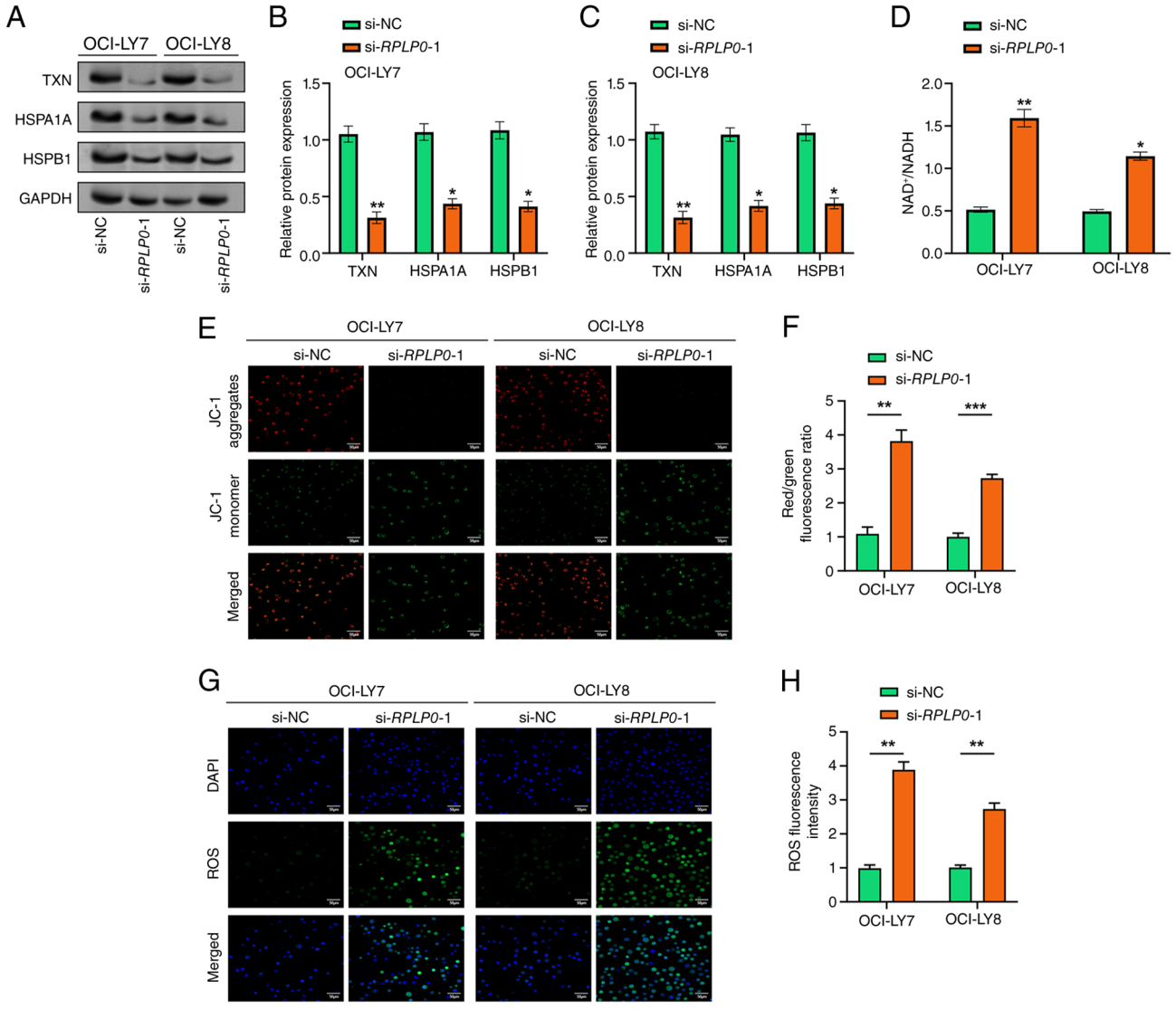

Figure 4. Effects of *RPLP0* knockdown on oxidative stress and mitochondrial function in OCI-LY7 and OCI-LY8 cell lines. (A) Representative western blotting images showing the expression of TXN, HSPA1A and HSPB1 in OCI-LY7 and OCI-LY8 cells following *RPLP0* knockdown. GAPDH was used as the loading control. (B) Quantitative analysis of TXN, HSPA1A and HSPB1 protein expression in OCI-LY7 cells. (C) Quantitative analysis of TXN, HSPA1A and HSPB1 protein expression in OCI-LY8 cells. (D) Measurement of the NAD^+/NADH ratio in OCI-LY7 and OCI-LY8 cells following si-*RPLP0*-1 transfection. The x-axis represents the treatment groups (si-NC vs. si-*RPLP0*-1) and the y-axis shows the NAD^+/NADH ratio. (E) Mitochondrial membrane potential analysis by JC-1 staining in *RPLP0*-knockdown OCI-LY7 and OCI-LY8 cell. Scale bar: 50 μm. (F) Quantitative analysis of the JC-1 red/green fluorescence ratio. (G) ROS levels in OCI-LY7 and OCI-LY8 cells following si-*RPLP0*-1 transfection, measured by 7'-dichlorodihydrofluorescein diacetate fluorescence. Scale bar, 50 μm. (H) Quantitative analysis of relative reactive oxygen species fluorescence intensity. *P<0.05, **P<0.01 and ***P<0.001. ROS, reactive oxygen species; si, small interfering RNA; NC, negative control; RPLP0, ribosomal protein lateral stalk subunit P0; TXN, thioredoxin; HSPA1A, heat shock protein family A member 1A; HSPB1, heat shock protein family B member 1.

mTOR were examined by WB analysis. The present findings indicated that although there were no appreciable changes in the overall expression levels of AKT and mTOR, *RPLP0* overexpression increased the levels of p-AKT and p-mTOR (Fig. 6D-F). According to these data, *RPLP0* may trigger the AKT/mTOR pathway in DLBCL cells. The impact of *RPLP0* overexpression and the mTOR inhibitor RAPA (25 nM) on LC3 and ATG5 expression in OCI-LY7 and OCI-LY8 cells was further investigated. The present results demonstrated that *RPLP0* overexpression reduced the LC3-II/I ratio and decreased ATG5 levels. However, co-treatment with RAPA partially reversed these effects, markedly restoring the LC3-II/I ratio and ATG5 protein levels (Fig. 6G-I). These results indicate that *RPLP0* overexpression activates the AKT/mTOR pathway, thereby inhibiting stress-induced autophagy in DLBCL cells.

RPLP0 modulates ROS-induced AKT/mTOR signaling and autophagy in DLBCL cells. NAC is a well-known ROS scavenger that specifically reduces intracellular ROS levels by directly reacting with ROS in redox reactions. To explore the role of *RPLP0* in ROS regulation and its impact on downstream signaling, the authors investigated the effects of *RPLP0* knockdown and NAC treatment (5 mM) on the AKT/mTOR signaling pathway in OCI-LY7 and OCI-LY8 cell lines. *RPLP0* knockdown notably decreased p-AKT and p-mTOR, according to WB analysis. However, upon NAC treatment, the levels of p-AKT and p-mTOR were restored

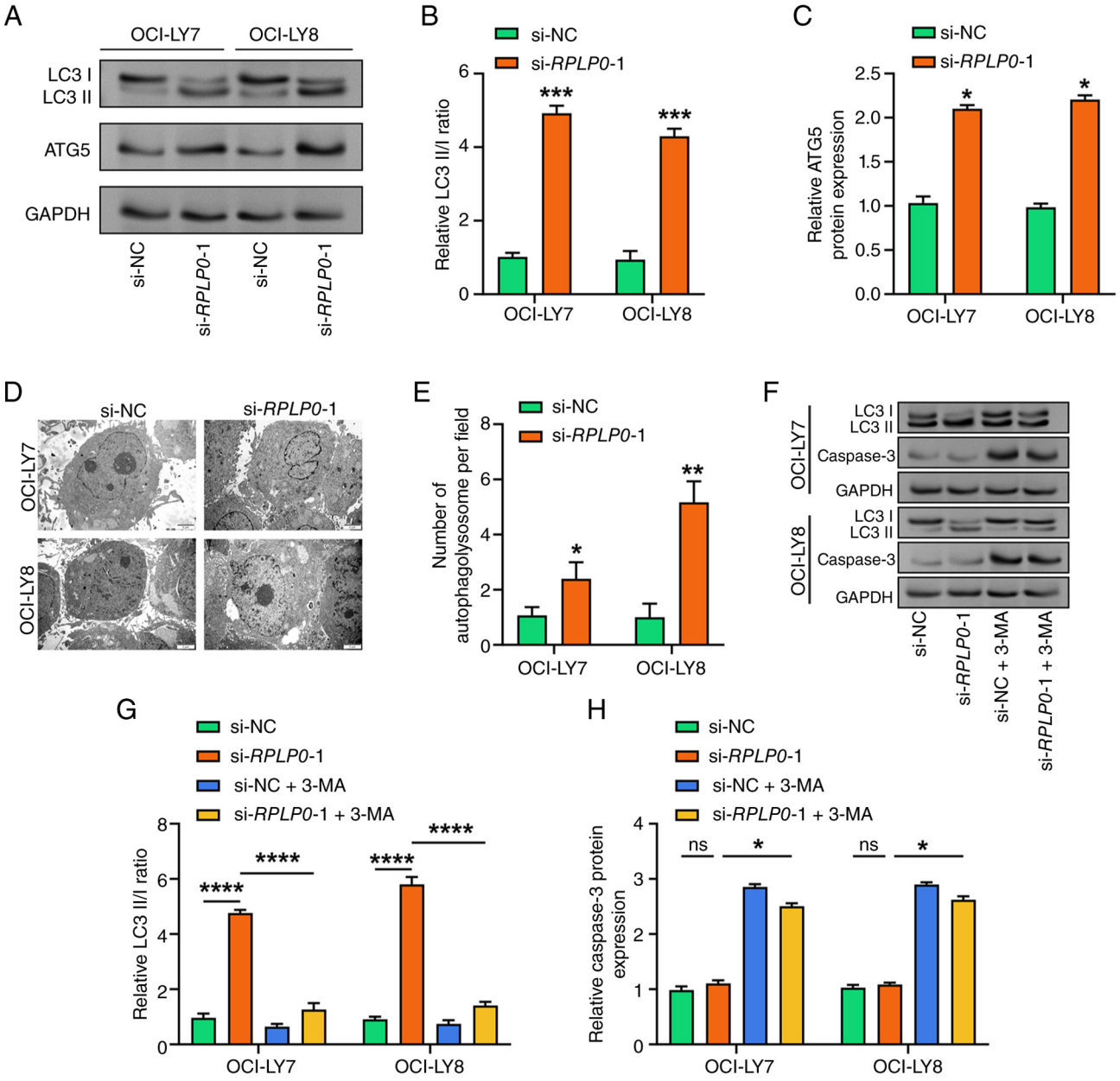

Figure 5. Impact of *RPLP0* knockdown on autophagy markers, mitochondrial morphology and the effects of 3-MA treatment in OCI-LY7 and OCI-LY8 cells. (A) WB analysis of autophagy-related proteins LC3 and ATG5 in OCI-LY7 and OCI-LY8 cells transfected with si-*RPLP0*-1. (B) Quantitative analysis of the LC3-II/LC3-I ratio in OCI-LY7 and OCI-LY8 cells. (C) Quantitative analysis of ATG5 protein expression in OCI-LY7 and OCI-LY8 cells. (D) Transmission electron microscopy images showing increased autophagic vacuoles in *RPLP0*-silenced cells compared with controls, with (E) quantitative analysis of the number of autolysosomes per field. Scale bar, 2 μm. (F) WB analysis of LC3-I, LC3-II, cleaved Caspase-3 and Caspase-3 expression in OCI-LY7 and OCI-LY8 cells treated with 3-MA (5 mM) following si-*RPLP0*-1 transfection. (G) Quantitative analysis of the LC3-II/LC3-I ratio in the indicated treatment groups. (H) Quantitative analysis of Caspase-3 protein expression in the indicated treatment groups. *P<0.05, **P<0.01, ***P<0.001, ****P<0.0001 and ns, not significant. WB, western blotting; 3-MA, 3-methyladenine; *RPLP0*, ribosomal protein lateral stalk subunit P0; si, small interfering RNA; NC, negative control; ATG5, autophagy-related gene 5.

to control levels, while the total protein expression of AKT and mTOR remained unaffected (Fig. 7A-C). The WB findings then demonstrated that *RPLP0* knockdown increased the LC3-II/I ratio and ATG5 expression. Following NAC therapy, ATG5 expression returned to baseline, and the LC3-II/I ratio normalized (Fig. 7D-F). Additionally, the CCK-8 assay was employed to measure cell viability. The present results showed that NAC therapy could restore the considerable decline in cell viability caused by *RPLP0* knockdown (Fig. 7G and H). According to these findings, *RPLP0* controls the buildup of ROS in DLBCL, thereby activating the AKT/mTOR signaling pathway and preventing oxidative stress-induced autophagy.

Discussion

By combining TCGA-DLBCL and GSE12453 datasets, 396 overlapping upregulated genes were found. Six ribosome-related candidate genes (*RPSI*1, *RPL27*, *RPSI8*, *RPS5*, *RPLP0* and *RPS3*) were found to be markedly differentially expressed in DLBCL

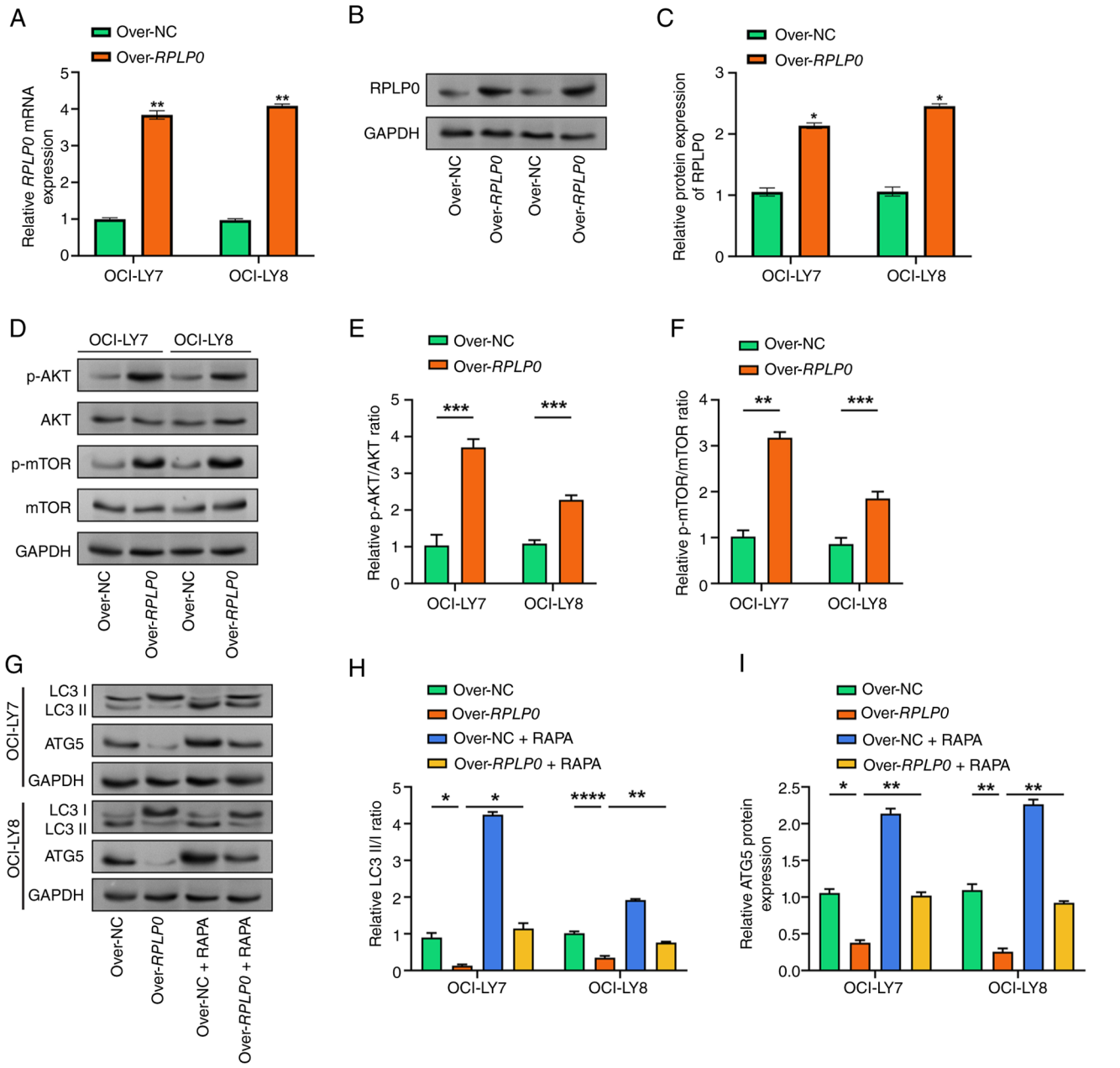

Figure 6. Effects of *RPLP0* overexpression on the AKT/mTOR pathway and autophagy in OCI-LY7 and OCI-LY8 cell lines. (A) RT-qPCR analysis of *RPLP0* expression in OCI-LY7 and OCI-LY8 cells transfected with the *RPLP0* overexpression plasmid. The x-axis represents the treatment groups, and the y-axis shows relative mRNA expression levels. (B) WB analysis of *RPLP0* expression in OCI-LY7 and OCI-LY8 cells transfected with the *RPLP0* overexpression plasmid. (C) Quantitative analysis of RPLP0 protein expression in OCI-LY7 and OCI-LY8 cells. (D) Representative WB images showing the expression of phosphorylated AKT, total AKT, phosphorylated mTOR and total mTOR in OCI-LY7 and OCI-LY8 cells following *RPLP0* overexpression. GAPDH was used as the loading control. (E) Quantitative analysis of the phosphorylated AKT/total AKT ratio. (F) Quantitative analysis of the phosphorylated mTOR/total mTOR ratio. (G) Representative WB images showing LC3-I, LC3-II and ATG5 expression in OCI-LY7 and OCI-LY8 cells following *RPLP0* overexpression, with or without RAPA treatment (25 nM). GAPDH was used as the loading control. (H) Quantitative analysis of the LC3-II/LC3-I ratio in the indicated treatment groups. (I) Quantitative analysis of ATG5 protein expression in the indicated treatment groups. *P<0.05, **P<0.01, ***P<0.001 and ****P<0.0001. RT-qPCR, reverse transcription-quantitative PCR; RAPA; rapamycin, WB, western blotting; ATG5, autophagy-related gene 5.

based on PPI network analysis. Experiments on cellular function revealed that *RPLP0* knockdown reduced cell survival and colony-forming capacity. Concurrently, *RPLP0* knockdown altered the cell cycle distribution, decreasing S phase and increasing G_2 phase accumulation, whereas apoptosis levels remained constant. Mechanistically, *RPLP0* knockdown caused mitochondrial depolarization, elevated intracellular ROS levels and disrupted redox equilibrium. *RPLP0* knockdown caused autophagy (LC3-II accumulation and ATG5 overexpression) and decreased the levels of oxidative stress-related proteins (TXN, HSPA1A and HSPB1). Conversely, *RPLP0* overexpression reduced autophagy markers and increased AKT/mTOR phosphorylation, which RAPA partially reversed. Importantly, scavenging ROS with NAC restored AKT/mTOR activity, normalized autophagy-related proteins and rescued the viability of *RPLP0*-silenced cells. These results indicate that *RPLP0* promotes DLBCL cell survival by coordinating the ROS-dependent AKT/mTOR signaling pathway to limit stress-induced autophagy.

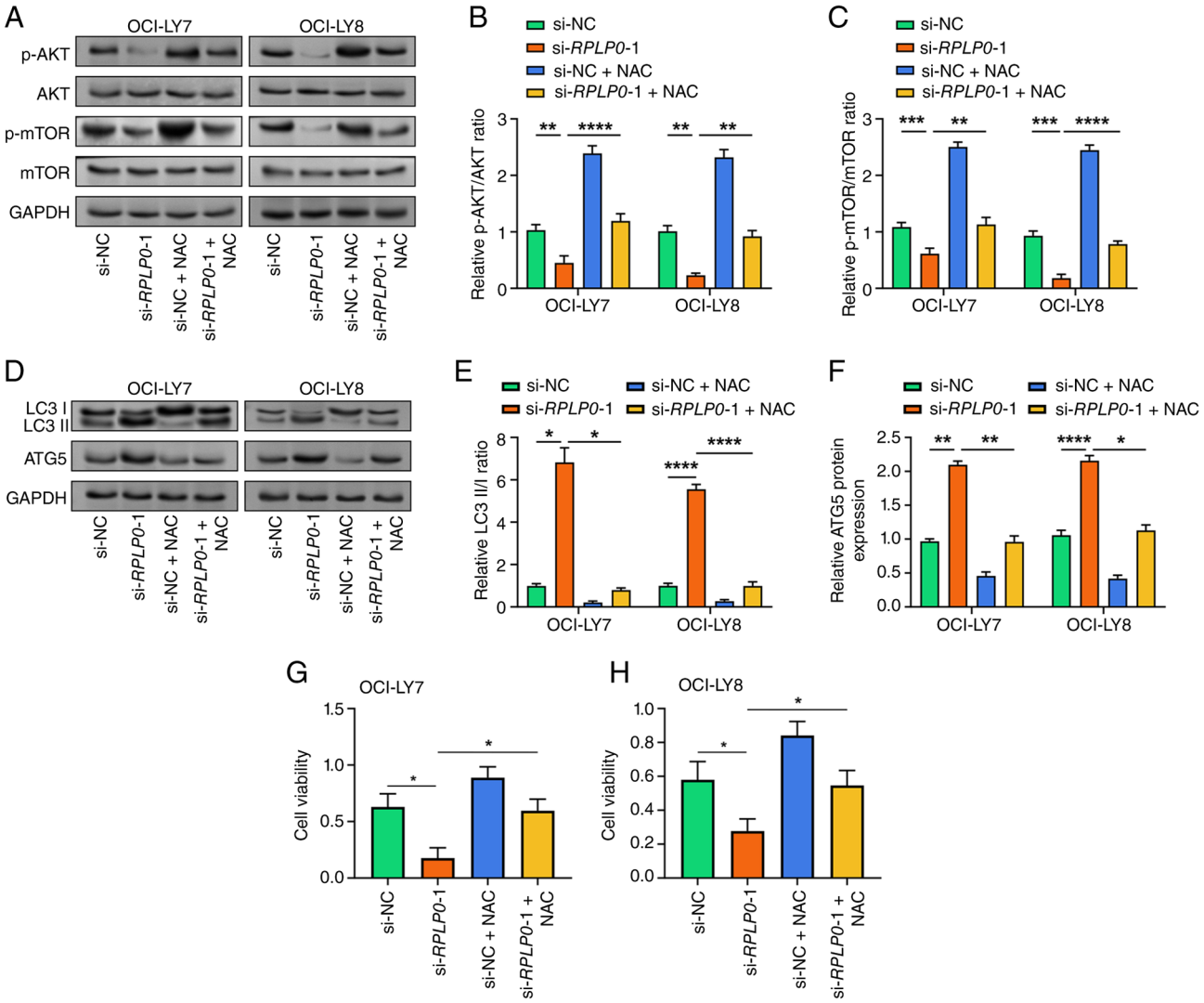

Figure 7. Effects of *RPLP0* knockdown and NAC treatment on AKT/mTOR signaling, autophagy, and cell viability in DLBCL cell lines. (A) Representative WB images and quantitative analysis of AKT/mTOR pathway-related proteins in OCI-LY7 and OCI-LY8 cells after *RPLP0* knockdown, with or without NAC treatment (5 mM). (B) Quantitative analysis of the phosphorylated AKT/total AKT ratio in the indicated treatment groups. (C) Quantitative analysis of the phosphorylated mTOR/total mTOR ratio in the indicated treatment groups. (D) Representative WB images and quantitative analysis of LC3 and autophagy-related gene 5 expression in OCI-LY7 and OCI-LY8 cells after *RPLP0* knockdown, with or without NAC treatment. (E) Quantitative analysis of the LC3-II/LC3-I ratio in the indicated treatment groups. (F) Quantitative analysis of autophagy-related protein 5 expression in the indicated treatment groups. (G and H) Cell viability analysis using CCK-8 assays in (G) OCI-LY7 and (H) OCI-LY8 cells following *RPLP0* knockdown and NAC treatment. The x-axis represents the treatment groups, and the y-axis shows relative cell viability. *P<0.05, **P<0.01, ***P<0.001 and ****P<0.0001. DLBCL, diffuse large B-cell lymphoma; WB, western blot; NAC, N-acetyl-L-cysteine; CCK-8, Cell Counting Kit-8; RPLP0, ribosomal protein lateral stalk subunit P0; si, small interfering RNA; NC, negative control; p-, phosphorylated.

DLBCL is a highly aggressive malignant tumor characterized by rapid proliferation and immense biosynthetic demands; therefore, ribosome biogenesis and protein translation are important for maintaining malignant growth (27). Consistent with this, ribosomal gene signatures have shown prognostic value in DLBCL, providing a basis for risk stratification and potential therapeutic targets. A previous study supports the functional relevance of ribosomal proteins in the biology of DLBCL. *RPS6* is upregulated in DLBCL, and its knockdown suppresses proliferation (28). Low-dose RAPA modulates *5'TOP* mRNA translation, a process regulated by *RPS6*, linking *RPS6* to aberrant protein synthesis in DLBCL. In the present study, the authors integrated DLBCL-related datasets and identified six consistently upregulated ribosome-related candidate genes (*RPS11*, *RPL27*, *RPS18*, *RPS5*, *RPLP0* and *RPS3*). Although these genes have not yet been fully studied in DLBCL, cumulative evidence from other malignancies highlights their pro-tumorigenic potential. For example, aberrant upregulation of *RPS3* has been linked to cancer progression and treatment resistance through the NF-κB pathway, while *RPL27* has been reported to promote colorectal cancer progression; its depletion impairs cell cycle progression and cell proliferation and attenuates the malignant phenotype (29,30). Notably, *RPLP0* is also associated with different cancers, including cervical cancer, breast cancer, lung adenocarcinoma and gastric cancer, with high expression correlating with tumorigenesis and poor prognosis (31-33). A mechanistic study suggests that the upstream tumor suppressor phospholipase A and acyltransferase 4 can regulate *RPLP0* to inhibit proliferation and survival, and may regulate key cell cycle checkpoints

through CDK2 and p21-related pathways (34). Consistent with these observations, the present data show that *RPLP0* is notably upregulated in DLBCL cells, and its knockdown inhibits proliferation and induces G_2 phase arrest, supporting *RPLP0* as a potentially clinically relevant functional hub gene in DLBCL.

ROS serve a regulatory role in cellular activity, but excessive levels can lead to oxidative stress, which damages cellular structure and function (35). Modulating ROS may be a potential treatment approach for DLBCL, as the loss of mitochondrial membrane potential during apoptosis is frequently accompanied by elevated ROS levels (36). To preserve intracellular redox homeostasis, TXN is a crucial redox-regulating protein (37). Classic indicators of heat shock and protein toxicity stress, HSPA1A and HSPB1, can prevent irreversible protein aggregation under stressful conditions (38,39). According to Feng *et al* (40) DCZ0358 suppresses cell growth and induces G_0/G_1 cell cycle arrest in DLBCL by impairing mitochondrial function and increasing ROS levels. The JNK signaling pathway is then triggered, encouraging apoptosis. Additionally, prior research has demonstrated that downregulation of ribosomal P complex proteins (such as RPLP0, RPLP1 or RPLP2) results in the buildup of ROS, which in turn causes endoplasmic reticulum stress and the unfolded protein response, ultimately triggering autophagy (41). According to research by Meng *et al* (42) *RPLP0* is overexpressed in hepatocellular carcinoma (HCC) and is associated with a bad prognosis. *RPLP0* regulates the ROS-JAK2/STAT3-c-Myc pathway, forming a positive feedback loop with c-Myc to promote HCC progression. Consistent with these observations, the present data demonstrate that *RPLP0* knockdown in DLBCL downregulates TXN, HSPA1A and HSPB1, thereby altering the cellular redox state and elevating the NAD^+/NADH ratio. Additionally, *RPLP0* knockdown causes mitochondrial depolarization, which eventually results in a large build-up of ROS. Notably, despite these pro-apoptotic signals, apoptosis remained unchanged, which the authors attribute to concurrent activation of protective autophagy, which buffers against cell death, as supported by 3-MA and NAC experiments. In conclusion, the present results imply that *RPLP0* serves an essential role in maintaining redox homeostasis and mitochondrial integrity in DLBCL cells and may be a potential therapeutic target.

A number of studies have shown that autophagy reduces oxidative stress by eliminating damaged mitochondria, thereby averting oxidative stress-induced cellular damage (43,44). According to Zhang *et al* (45) patients with DLBCL had considerably higher levels of the autophagy marker p62 than those with reactive lymphoid hyperplasia, and higher p62 expression was associated with a shorter 2-year progression-free survival. Chen *et al* (46) demonstrated that artesunate (ART) induces autophagy, ferroptosis, apoptosis and cell cycle arrest in DLBCL cells by blocking the STAT3 signaling pathway. Furthermore, ART-induced apoptosis was mitigated by suppression of autophagy and ferroptosis, underscoring the complex interactions between these cellular mechanisms. To engage in autophagy, LC3, a crucial protein on the autophagosome membrane, changes from LC3-I to LC3-II (47). ATG5 promotes the development and growth of the autophagosomal membrane by interacting with ATG12 and ATG16L1 (48). In the present investigation, *RPLP0* knockdown in DLBCL cells increased ATG5 expression and elevated the LC3-II/I ratio. TEM revealed an increased number of autophagosomes, suggesting activation of autophagy. Furthermore, treatment with the autophagy inhibitor 3-MA markedly reduced the LC3-II/I ratio. These outcomes suggest that *RPLP0* deficiency may control autophagy, which may help DLBCL cells manage oxidative stress and mitochondrial malfunction.

The PI3K/AKT/mTOR signaling pathway is a well-known regulatory system for autophagy that is key for several biological processes (49). Studies have shown that the loss of ribosomal proteins reduces mTOR phosphorylation in cancer cells, thereby affecting autophagy and the regulation of proliferation (50,51). According to research by Wang *et al* (52) research, macrophage-capping protein is upregulated in DLBCL and activates the PI3K/AKT signaling pathway to promote cell invasion and proliferation. Similarly, Li *et al* (53) noted that in pancreatic ductal adenocarcinoma, ROS activate AMPK to trigger autophagy while inhibiting mTORC1. The authors' research demonstrates that tailored selective autophagy can reduce the risk of adverse effects. Du *et al* (54) found that plumbagin (PL) increased ROS generation and inhibited the growth of DLBCL cells. Additionally, PL decreased the expression of p-Akt, p-PI3K, Bcl-2 and p-mTOR while increasing the expression of cleaved Caspase-3 and Bax. These findings suggest that PL induces apoptosis in DLBCL cells by triggering oxidative stress, which in turn inactivates the PI3K/AKT/mTOR signal pathway. In the present study, *RPLP0* overexpression was shown to activate the AKT/mTOR signaling pathway, thereby suppressing autophagy and increasing cell survival. Conversely, *RPLP0* knockdown increases autophagy, suppresses AKT/mTOR phosphorylation and causes ROS buildup in DLBCL cells. It is noteworthy that NAC can reverse alterations in autophagy and restore AKT/mTOR function. These findings emphasize the therapeutic promise of *RPLP0*, revealing its critical role in regulating cell survival in DLBCL by orchestrating the autophagy process, thereby modulating the AKT/mTOR signaling pathway.

Several limitations of the present study should be acknowledged. First, all functional experiments were performed only in DLBCL cell lines, without *in vivo* validation using animal models. Second, the present findings are primarily derived from cell-based assays and public database analyses and lack direct validation with independent clinical DLBCL specimens. Third, the present study did not investigate whether *RPLP0* exerts differential effects across other DLBCL subtypes, as only germinal center B-cell-like-subtype cell lines were used. Future studies will establish DLBCL xenograft mouse models, validate *RPLP0* expression and its clinical relevance using larger patient cohorts, and explore its subtype-specific roles using additional cell lines and clinical samples from different molecular subtypes.

In conclusion, the present research examined the vital role of *RPLP0* in controlling autophagy, mitochondrial activity and oxidative stress in DLBCL. Functional studies demonstrated that *RPLP0* knockdown led to G_2 cell cycle arrest and reduced cell growth. By controlling mitochondrial function, *RPLP0* knockdown also made oxidative stress worse in DLBCL. Additionally, *RPLP0* overexpression can

stimulate the AKT/mTOR signaling pathway and suppress autophagy in DLBCL cells, whereas *RPLP0* deficiency can enhance autophagy. Notably, by triggering the ROS-induced AKT/mTOR signaling pathway, *RPLP0* markedly contributes to the survival of DLBCL cells under oxidative stress. These discoveries may guide the development of therapies targeting the *RPLP0*-related pathway and deepen understanding of DLBCL.

Acknowledgements

Not applicable.

Funding

No funding was received.

Availability of data and materials

The data generated in the present study may be requested from the corresponding author.

Authors' contributions

Conception and design of the research was performed by SW, XY and JT. Acquisition of data was performed by SW and XY. Analysis and interpretation of data was the responsibility of SW, XY, RM, BH, DS and NM. RM, BH, SS and NM performed the statistical analysis. SW and XY drafted the manuscript. JT revised the manuscript for important intellectual content. All authors have read and approved the final version of the manuscript. SW and XY confirm the authenticity of all the raw data.

Ethics approval and consent to participate

Not applicable.

Patient consent for publication

Not applicable.

Competing interests

The authors declare that they have no competing interests.

Use of artificial intelligence tools

During the preparation of this work, artificial intelligence tools were used to improve the readability and language of the manuscript or to generate images, and subsequently, the authors revised and edited the content produced by the artificial intelligence tools as necessary, taking full responsibility for the ultimate content of the present manuscript.

References

1. Shi X, Zhuo H, Du Y, Nyhan K, Ioannidis J and Wallach JD: Environmental risk factors for non-Hodgkin's lymphoma: Umbrella review and comparison of meta-analyses of summary and individual participant data. BMJ Med 1: e000184, 2022.
2. Chu Y, Liu Y, Fang X, Jiang Y, Ding M, Ge X, Yuan D, Lu K, Li P, Li Y, *et al*: The epidemiological patterns of non-Hodgkin lymphoma: Global estimates of disease burden, risk factors, and temporal trends. Front Oncol 13: 1059914, 2023.
3. Mafra A, Laversanne M, Gospodarowicz M, Klinger P, De Paula Silva N, Piñeros M, Piñeros M, Steliarova-Foucher E, Bray F and Znaor A: Global patterns of non-Hodgkin lymphoma in 2020. Int J Cancer 151: 1474-1481, 2022.
4. Garg M, Takyar J, Dhawan A, Saggu G, Agrawal N, Hall A, Raut M and Ryland KE: Diffuse large B-cell lymphoma (DLBCL): A structured literature review of the epidemiology, treatment guidelines, and real-world treatment patterns. Blood 140 (Suppl 1): S12106-S12107, 2022.
5. Berhan A, Almaw A, Damtie S and Solomon Y: Diffuse large B cell lymphoma (DLBCL): Epidemiology, pathophysiology, risk stratification, advancement in diagnostic approaches and prospects: Narrative review. Discov Oncol 16: 184, 2025.
6. He MY and Kridel R: Treatment resistance in diffuse large B-cell lymphoma. Leukemia 35: 2151-2165, 2021.
7. Walker JS, Wenzl K, Novak JP, Stokes ME, Hopper MA, Dropik AR, Siminski MS, Bock AM, Sarangi V, Ortiz M, *et al*: Integrated genomics with refined cell-of-origin subtyping distinguishes subtype-specific mechanisms of treatment resistance and relapse in diffuse large B-cell lymphoma. Blood Cancer J 15: 120, 2025.
8. Candelaria M and Dueñas-Gonzalez A: Rituximab in combination with cyclophosphamide, doxorubicin, vincristine, and prednisone (R-CHOP) in diffuse large B-cell lymphoma. Ther Adv Hematol 12: 2040620721989579, 2021.
9. Susanibar-Adaniya S and Barta SK: 2021 Update on diffuse large B cell lymphoma: A review of current data and potential applications on risk stratification and management. Am J Hematol 96: 617-629, 2021.
10. Vietri M, Miranda MR, Amodio G, Ciaglia T, Bertamino A, Campiglia P, Remondelli P, Vestuto V and Moltedo O: The link between endoplasmic reticulum stress and lysosomal dysfunction under oxidative stress in cancer cells. Biomolecules 15: 930, 2025.
11. Zuo H, Chen C and Sa Y: Therapeutic potential of autophagy in immunity and inflammation: Current and future perspectives. Pharmacol Rep 75: 499-510, 2023.
12. Xu H, Yu X, Yang Z, Song Q, Cheng S, He Z and Dai L: PAX5-activated lncRNA ARRDC1-AS1 accelerates the autophagy and progression of DLBCL through sponging miR-2355-5p to regulate ATG5. Life Sci 286: 119932, 2021.
13. Kong YL, Pan BH, Liang JH, Zhu HY, Wang L, Xia Y, Wu JZ, Fan L, Li JY and Xu W: Chidamide, a histone deacetylase inhibitor, inhibits autophagy and exhibits therapeutic implication in chronic lymphocytic leukemia. Aging (Albany NY) 12: 16083-16098, 2020.
14. Mouhssine S, Maher N, Matti BF, Alwan AF and Gaidano G: Targeting BTK in B cell malignancies: From mode of action to resistance mechanisms. Int J Mol Sci 25: 3234, 2024.
15. Yan B, Guo J, Lai W, Chen Y, Wang Z, Peng Y and Chang S: The multifaceted roles of ribosomal P complex in cancer. World J Surg Oncol 23: 388, 2025.
16. Chang C and Xu M: miR-4731-5p enhances apoptosis and alleviates epithelial-mesenchymal transition through targeting RPLP0 in non-small-cell lung cancer. J Oncol 2022: 3793318, 2022.
17. Pérez-Gómez JM, Porcel-Pastrana F, De La Luz-Borrero M, Montero-Hidalgo AJ, Gómez-Gómez E, Herrera-Martínez AD, Guzmán-Ruiz R, Malagón MM, Gahete MD and Luque RM: LRP10, PGK1 and RPLP0: Best reference genes in periprostatic adipose tissue under obesity and prostate cancer conditions. Int J Mol Sci 24: 15140, 2023.
18. Zhou J, Li XY, Liu YJ, Feng J, Wu Y, Shen HM and Lu GD: Full-coverage regulations of autophagy by ROS: From induction to maturation. Autophagy 18: 1240-1255, 2022.
19. Omolekan TO, Chamcheu JC, Buerger C and Huang S: PI3K/AKT/mTOR signaling network in human health and diseases. Cells 13: 1500, 2024.
20. Gomez Solsona B, Horn H, Schmitt A, Xu W, Bucher P, Heinrich A, Kalmbach S, Kreienkamp N, Franke M, Wimmers F, *et al*: Inhibition of glutaminase-1 in DLBCL potentiates venetoclax-induced antitumor activity by promoting oxidative stress. Blood Adv 7: 7433-7444, 2023.
21. Caserta S, Martino EA, Skafi M, Alvaro ME, Bruzzese A, Amodio N, Lucia E, Olivito V, Labanca C, Mendicino F, *et al*: Management of primary refractory diffuse large B-cell lymphoma in patients unsuitable for CAR T-cell therapy. Eur J Haematol 116: 771-784, 2026.

22. Brune V, Tiacci E, Pfeil I, Döring C, Eckerle S, Van Noesel CJ, Klapper W, Falini B, von Heydebreck A, Metzler D, *et al*: Origin and pathogenesis of nodular lymphocyte-predominant Hodgkin lymphoma as revealed by global gene expression analysis. J Exp Med 205: 2251-2268, 2008.
23. Ritchie ME, Phipson B, Wu D, Hu Y, Law CW, Shi W and Smyth GK: limma powers differential expression analyses for RNA-sequencing and microarray studies. Nucleic Acids Res 43: e47, 2015.
24. Hata A and Hayama M: Selection of RT-PCR assays and reliability of viral gene detection in water samples containing RT-PCR inhibitors. Water Air Soil Pollut 236: 618, 2025.
25. Livak KJ and Schmittgen TD: Analysis of relative gene expression data using real-time quantitative PCR and the 2(-Delta Delta C(T)) method. Methods 25: 402-408, 2001.
26. Xiang Y, Zheng Y, Liu S, Liu G, Li Z and Dong W: Comparison of the sensitivity of western blotting between PVDF and NC membranes. Sci Rep 11: 12022, 2021.
27. Bram Ednersson S, Stenson M, Stern M, Enblad G, Fagman H, Nilsson-Ehle H, Hasselblom S and Andersson PO: Expression of ribosomal and actin network proteins and immunochemotherapy resistance in diffuse large B cell lymphoma patients. Br J Haematol 181: 770-781, 2018.
28. Hagner PR, Mazan-Mamczarz K, Dai B, Balzer EM, Corl S, Martin SS, Zhao XF and Gartenhaus RB: Ribosomal protein S6 is highly expressed in non-Hodgkin lymphoma and associates with mRNA containing a 5' terminal oligopyrimidine tract. Oncogene 30: 1531-1541, 2011.
29. Liang ZX, Liu HS, Xiong L, Yang X, Wang FW, Zeng ZW, He XW, Wu XR and Lan P: A novel NF-κB regulator encoded by circPLCE1 inhibits colorectal carcinoma progression by promoting RPS3 ubiquitin-dependent degradation. Mol Cancer 20: 103, 2021.
30. Park SY, Seo D, Jeon EH, Park JY, Jang BC, Kim JI, Im SS, Lee JH, Kim S, Cho CH and Lee YH: RPL27 contributes to colorectal cancer proliferation and stemness via PLK1 signaling. Int J Oncol 63: 93, 2023.
31. Xu C, Lu Z, Hou G and Zhu M: Exploring the function and prognostic value of RPLP0, RPLP1 and RPLP2 expression in lung adenocarcinoma. J Mol Histol 55: 1079-11091, 2024.
32. Teller A, Jechorek D, Hartig R, Adolf D, Reißig K, Roessner A and Franke S: Dysregulation of apoptotic signaling pathways by interaction of RPLP0 and cathepsin X/Z in gastric cancer. Pathol Res Pract 211: 62-70, 2015.
33. Lin D, Fu R, Xi E and Bai Y (eds): Computational prediction of biological signatures for candidate driver genes associated with ovarian cancer. 2021 IEEE International Conference on Bioinformatics and Biomedicine (BIBM). IEEE, 2021.
34. Wang CH, Wang LK, Wu CC, Chen ML, Lee MC, Lin YY and Tsai FM: The ribosomal protein RPLP0 mediates PLAAT4-induced cell cycle arrest and cell apoptosis. Cell Biochem Biophys 77: 253-260, 2019.
35. Murphy MP, Bayir H, Belousov V, Chang CJ, Davies KJA, Davies MJ, Dick TP, Finkel T, Forman HJ, Janssen-Heininger Y, *et al*: Guidelines for measuring reactive oxygen species and oxidative damage in cells and in vivo. Nat Metab 4: 651-662, 2022.
36. Wu C, Chen S, Wu Z, Xue J, Zhang W, Wang S, Zhao X and Wu S: Chidamide and orelabrutinib synergistically induce cell cycle arrest and apoptosis in diffuse large B-cell lymphoma by regulating the PI3K/AKT/mTOR pathway. J Cancer Res Clin Oncol 150: 98, 2024.
37. Muri J and Kopf M: The thioredoxin system: Balancing redox responses in immune cells and tumors. Eur J Immunol 53: e2249948, 2023.
38. Kumari B: Cellular stress responses and associated diseases: A focus on heat shock proteins. Cell Biochem Biophys 83: 2793-2804, 2025.
39. Bonavita R, Vitale F, Verdicchio LV, Williams SV, Caporaso MG, Fleming A and Renna M: Small HSPs at the crossroad between protein aggregation, autophagy and unconventional secretion: Clinical implications and potential therapeutic opportunities in the context of neurodegenerative diseases. Front Cell Dev Biol 13: 1538377, 2025.
40. Feng Q, Hu K, Hu H, Lu Y, Zhang H, Wang G, Zhang Q, Xu Z, Gao X, Jia X, *et al*: Berberine derivative DCZ0358 induce oxidative damage by ROS-mediated JNK signaling in DLBCL cells. Int Immunopharmacol 125: 111139, 2023.
41. Du X, Wei H, Zhang B, Pang LK, Zhao R, Zhang XD and Yao W: Unveiling the prognostic implications of RPLP1 upregulation in osteosarcoma. Am J Cancer Res 13: 4822-4831, 2023.
42. Meng Y, Yuan L, Meng G, Huang H, Huang X, Xu X and Peng X: c-Myc-regulated RPLP0 via the ROS-mediated JAK2/STAT3 positive feedback loop facilitates hepatocellular carcinoma malignancy progression. Int J Oncol 68: 13, 2026.
43. Liu X, Hussain R, Mehmood K, Tang Z, Zhang H and Li Y: Mitochondrial-endoplasmic reticulum communication-mediated oxidative stress and autophagy. Biomed Res Int 2022: 6459585, 2022.
44. Prakash R, Fauzia E, Siddiqui AJ, Yadav SK, Kumari N, Shams MT, Naeem A, Praharaj PP, Khan MA, Bhutia SK, *et al*: Oxidative stress-induced autophagy compromises stem cell viability. Stem Cells 40: 468-478, 2022.
45. Zhang YL, Ma MX, Xing LN, Zhang JN, Guo XN and Qiao SK: Downregulation of autophagy is associated with poor clinical outcome after immunochemotherapy in patients with diffuse large B-cell lymphoma. Exp Hematol 139: 104638, 2024.
46. Chen Y, Wang F, Wu P, Gong S, Gao J, Tao H, Shen Q, Wang S, Zhou Z and Jia Y: Artesunate induces apoptosis, autophagy and ferroptosis in diffuse large B cell lymphoma cells by impairing STAT3 signaling. Cell Signal 88: 110167, 2021.
47. Iriondo MN, Etxaniz A, Varela YR, Ballesteros U, Hervás JH, Montes LR, Goñi FM and Alonso A: LC3 subfamily in cardiolipin-mediated mitophagy: A comparison of the LC3A, LC3B and LC3C homologs. Autophagy 18: 2985-3003, 2022.
48. Wei F, Qin N, Chen Y, Liu Z, Zhao X, Yu X, Feng Z, Wang Y, Yang A and Cui H: ATG16L1 membrane recruitment in autophagy. Crit Rev Biochem Mol Biol 60: 107-122, 2025.
49. Huang J, Chen L, Wu J, Ai D, Zhang JQ, Chen TG and Wang L: Targeting the PI3K/AKT/mTOR signaling pathway in the treatment of human diseases: Current status, trends, and solutions. J Med Chem 65: 16033-16061, 2022.
50. Yi X, Zhang C, Liu B, Gao G, Tang Y, Lu Y, Pan Z, Wang G and Feng W: Ribosomal protein L22-like1 promotes prostate cancer progression by activating PI3K/Akt/mTOR signalling pathway. J Cell Mol Med 27: 403-411, 2023.
51. Liu L, Wu Y, Liu K, Zhu M, Guang S, Wang F, Liu X, Yao X, He J and Fu C: The absence of the ribosomal protein Rpl2702 elicits the MAPK-mTOR signaling to modulate mitochondrial morphology and functions. Redox Biol 73: 103174, 2024.
52. Wang G, Liu H, An L, Hou S and Zhang Q: CAPG facilitates diffuse large B-cell lymphoma cell progression through PI3K/AKT signaling pathway. Hum Immunol 83: 832-842, 2022.
53. Li J, Chen X, Kang R, Zeh H, Klionsky DJ and Tang D: Regulation and function of autophagy in pancreatic cancer. Autophagy 17: 3275-3296, 2021.
54. Du J, Ye T, Li P, Yu Y, Fan F, Zhang R and Shen N: Plumbagin induces apoptosis in diffuse large B-cell lymphoma by modulating the ROS-PI3K-Akt-mTOR signaling pathway. Crit Rev Eukaryot Gene Expr 35: 13-25, 2025.